Discriminating baryonium and final-state-interaction interpretations of $X(2356)$*

Bing-Dong Wan (万秉东)[1,2†] Sheng-Qi Zhang (张圣奇)[3‡]

[1]Department of Physics, Liaoning Normal University, Dalian 116029, China
[2]Center for Theoretical and Experimental High Energy Physics, Liaoning Normal University, Dalian 116029, China
[3]Center for High Energy Physics, Peking University, Beijing 100871, China

Abstract: We revisit the $X(2356)$ enhancement observed by BESIII in $e^+e^- \to \Lambda\bar{\Lambda}\eta$ from the perspective of near-threshold dynamics. Motivated by the possible existence of light $\Lambda\bar{\Lambda}$ baryonium, we compare this interpretation with final-state interaction (FSI) explanations within a minimal FSI-dressed pole framework. Fits of pure-FSI, baryonium-like-pole, and mixed pole–continuum scenarios to the digitized BESIII spectrum indicate that the energy-dependent FSI description achieves the best balance between fit quality and model complexity. The extracted pole positions depend strongly on the amplitude parametrization, highlighting the sensitivity of the baryonium interpretation to the treatment of the continuum. We discuss how decay channels, spin observables, and searches for partner states can provide complementary constraints on the dynamics underlying the enhancement.

Keywords: $X(2356)$, baryonium, final-state interaction, threshold enhancement, $\Lambda\bar{\Lambda}$

DOI: 10.1088/1674-1137/aeb2b2 **CSTR:** 32044.14.ChinesePhysicsC.51

CPC Accepted

I. INTRODUCTION

Baryon-antibaryon systems, historically termed "baryonium", provide a natural arena for testing multiquark dynamics in nonperturbative QCD. In the one-boson-exchange picture, the G-parity transformation relates baryon-baryon interactions to baryon-antibaryon interactions and can convert some of the short-range repulsion in the baryon-baryon sector into attraction in the baryon-antibaryon sector [1–3]. This mechanism has long motivated searches for $N\bar{N}$ baryonium-like states [4–16] and for their strange and heavy-flavor analogues [17–20].

The $\Lambda\bar{\Lambda}$ channel is particularly useful because the isoscalar Λ forbids diagonal one-pion exchange, and its weak decay is self-analyzing, allowing access to spin observables [21, 22]. A structure in this channel therefore probes short- and intermediate-range baryon-antibaryon dynamics in a manner complementary to the more familiar $p\bar{p}$ sector.

Recently, the BESIII collaboration reported an enhancement near the $\Lambda\bar{\Lambda}$ threshold in the process $e^+e^- \to \Lambda\bar{\Lambda}\eta$, which we denote as $X(2356)$ [23]. This structure has quantum numbers $J^{PC} = 1^{--}$, a mass of $(2356 \pm 7 \pm 17)$ MeV/c^2, and a width of $(304 \pm 28 \pm 54)$ MeV. A previous QCD sum-rule study of the $\Lambda\bar{\Lambda}$ system predicted a vector state in the relevant mass region [17], making the baryonium interpretation a well-motivated possibility. At the same time, baryon-antibaryon threshold enhancements can arise without introducing a new compact state. The well-known $p\bar{p}$ enhancement associated with the $X(1835)$ has been interpreted in terms of final-state-interaction (FSI) effects [24], and the near-threshold behavior of $e^+e^- \to \Lambda\bar{\Lambda}$ has also been described using $\Lambda\bar{\Lambda}$ FSI [25]. Most directly, Haidenbauer and Meißner described the $e^+e^- \to \eta\Lambda\bar{\Lambda}$ spectrum within the distorted-wave Born approximation using Jülich $\Lambda\bar{\Lambda}$ potentials constrained by $p\bar{p} \to \Lambda\bar{\Lambda}$ data. They demonstrated that FSI alone can reproduce the near-threshold mass dependence after applying an overall normalization [26]. Their analysis was primarily designed to establish the role of the $\Lambda\bar{\Lambda}$ interaction, whereas a comparative assessment of explicit-pole and pole–continuum amplitudes lay beyond its scope.

This Letter therefore does not attempt to establish $X(2356)$ as a pure baryonium state from its mass alone. Instead, we ask which observations can discriminate a baryonium-like pole from an enhancement driven mainly by

Received 3 July 2026; Accepted 29 September 2026; Accepted manuscript online 30 September 2026

* Supported in part by the National Natural Science Foundation of China (12547114, 12575106, 12325503, 12147214), and Specific Fund of Fundamental Scientific Research Operating Expenses for Undergraduate Universities in Liaoning Province (LJ212410165019)

† E-mail: wanbd@lnnu.edu.cn

‡ E-mail: shqzhang@pku.edu.cn

Content from this work may be used under the terms of the Creative Commons Attribution 3.0 licence. Any further distribution of this work must maintain attribution to the author(s) and the title of the work, journal citation and DOI. Article funded by SCOAP[3] and published under licence by Chinese Physical Society and the Institute of High Energy Physics of the Chinese Academy of Sciences and the Institute of Modern Physics of the Chinese Academy of Sciences and IOP Publishing Ltd

$\Lambda\bar{\Lambda}$ FSI. To address this question, we first formulate a minimal FSI-dressed pole framework whose limiting cases correspond to a pure FSI enhancement, a baryonium-like pole, and a mixed pole–continuum scenario. We then fit these alternatives to the digitized BESIII spectrum, compare their fit quality and pole structures, and assess what can be distinguished with the present data. Finally, we clarify the relation of the QCD sum-rule prediction to the bare-state parameter and the dressed pole, and discuss how decay channels, partner searches, and polarization observables can further test the baryonium interpretation.

II. NEAR-THRESHOLD DYNAMICS

The main limitation of a purely spectroscopic discussion is that a near-threshold enhancement does not necessarily imply a new state. In baryon–antibaryon systems, the production amplitude can be strongly modified by the interaction between the outgoing baryon and antibaryon. This point is well established from the $p\bar{p}$ threshold enhancement in J/ψ decays [24], the description of $e^+e^- \to \Lambda\bar{\Lambda}$ near threshold in terms of $\Lambda\bar{\Lambda}$ final-state interactions [25], and the dynamical treatment of $e^+e^- \to \eta\Lambda\bar{\Lambda}$ and $e^+e^- \to \phi\Lambda\bar{\Lambda}$ [26]. Thus, any baryonium interpretation of $X(2356)$ must account for the continuum interaction.

A compact way to express this issue is to factorize the short-distance production kernel and the low-energy $\Lambda\bar{\Lambda}$ scattering amplitude,

$$\mathcal{M}(s) = \mathcal{M}_0(s)\, F_{\Lambda\bar{\Lambda}}(s), \tag{1}$$

where $s = M^2_{\Lambda\bar{\Lambda}}$, and $\mathcal{M}_0$ varies slowly across the narrow threshold region. In an effective-range representation, one may write, schematically,

$$F_{\Lambda\bar{\Lambda}}(k) = \frac{1}{-1/a + (r_e/2)k^2 - \mathrm{i}k}, \tag{2}$$

with k denoting the relative momentum and a and r_e the complex scattering length and effective range, respectively. We take $k > 0$ on the upper edge of the physical cut above the $\Lambda\bar{\Lambda}$ threshold. The physical $\Lambda\bar{\Lambda}$ sheet and the second $\Lambda\bar{\Lambda}$ sheet correspond to $\mathrm{Im}\,k > 0$ and $\mathrm{Im}\,k < 0$, respectively. With $S = 1 + 2\mathrm{i}kF_{\Lambda\bar{\Lambda}}$, absorption requires $\mathrm{Im}[-1/a + (r_e/2)k^2] \le 0$ for real $k > 0$. A pole near threshold corresponds to a zero of the denominator after analytic continuation, whereas a non-pole FSI enhancement can still increase the spectrum through a large low-energy amplitude. This form also clarifies why a lineshape fit alone is not always sufficient: both a nearby pole and a strong attractive FSI can enhance the same mass region.

To make this distinction explicit within a minimal model, we evaluate the $\Lambda\bar{\Lambda}$ spectrum using the two amplitudes shown in Fig. 1. For the FSI-only curve, we use Eq. (2) with

$$a = (-1.0 - 0.8\mathrm{i})\ \mathrm{fm}, \qquad r_e = 1.5\ \mathrm{fm}, \tag{3}$$

and multiply $|F_{\Lambda\bar{\Lambda}}(k)|^2$ by the two-body phase-space factor $\rho_{\Lambda\bar{\Lambda}}(s) = 2k/\sqrt{s}$. These illustrative values are on the order of 1 fm and are neither fitted to the BESIII data nor matched to the interaction in Ref. [26]. For real r_e, the negative imaginary part of a satisfies the absorptive condition in the convention of Eq. (2). For the pole-like curve, we use a Flatté-inspired denominator with

$$M_R = 2.355\ \mathrm{GeV}, \quad \Gamma_R = 0.12\ \mathrm{GeV}, \quad g_{\Lambda\bar{\Lambda}} = 0.35\ \mathrm{GeV}^2, \tag{4}$$

where the imaginary part is defined as $M_R\Gamma_R + g_{\Lambda\bar{\Lambda}}\rho_{\Lambda\bar{\Lambda}}(s)$.

When an explicit baryonium bare pole is introduced, the amplitude can be written as

$$\mathcal{M}(s) = \mathcal{M}_{\mathrm{bg}}(s) + \frac{c_{\gamma^*\eta X}\, g_{X\Lambda\bar{\Lambda}}}{M_R^2 - s - \Sigma_{\Lambda\bar{\Lambda}}(s) - iM_R\Gamma_{\mathrm{inel}}(s)}, \tag{5}$$

where the self-energy $\Sigma_{\Lambda\bar{\Lambda}}$ dresses the bare pole through the near-threshold continuum. Equations (1)–(5) describe three scenarios: an FSI amplitude without an explicit bare state, an FSI-dressed baryonium-like pole, and a coherent mixture of continuum and pole contributions.

Figure 1 illustrates how both FSI and an explicit pole can generate a near-threshold enhancement. For the chosen parameters, the FSI spectrum rises from threshold

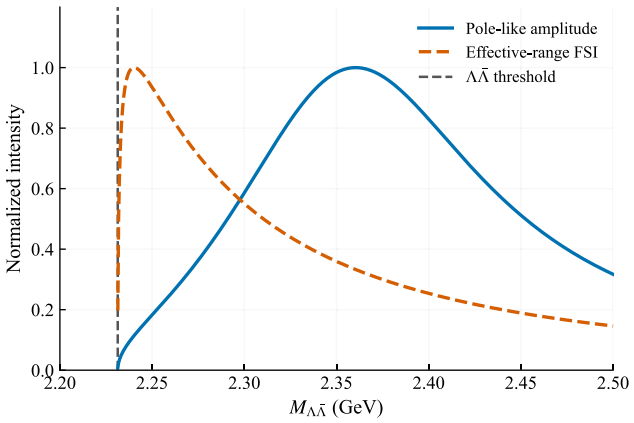


Fig. 1. (color online) Minimal-model comparison of a pole-like near-threshold enhancement with an FSI-only enhancement. The FSI-only curve uses the effective-range parameters in Eq. (3), whereas the pole-like curve uses the Flatté-inspired parameters in Eq. (4). Both spectra are normalized to their respective maxima. The vertical line marks the $\Lambda\bar{\Lambda}$ threshold.

CPC Accepted

to a nearby maximum and then decreases smoothly, whereas the pole-like spectrum exhibits a broader maximum at a higher mass. Section III examines whether the BESIII spectrum can distinguish between these scenarios using a common optical K-matrix parametrization and identical production and response factors.

III. QUANTITATIVE COMPARISON WITH THE DIGITIZED BESIII SPECTRUM

To determine whether the BESIII spectrum can discriminate among the three scenarios discussed above, we fit the black data points and the sideband curve digitized from Fig. 6 of Ref. [23]. The fit uses the 22 complete bins in $2.24 < M_{\Lambda\bar{\Lambda}} < 2.70$ GeV, with a common treatment of the response and background. Four fit variants represent the three physical scenarios: the pure-FSI case is described by constant and energy-dependent continuum amplitudes, whereas the baryonium-like and mixed cases are represented by an FSI-dressed bare pole and a coherent continuum–pole amplitude, respectively.

With $E = M_{\Lambda\bar{\Lambda}} - 2m_\Lambda$, $k = (M^2_{\Lambda\bar{\Lambda}}/4 - m^2_\Lambda)^{1/2}$, $C(E) = C_0 + C_1 E/\Lambda_E$, and $d(E) = E_0 - E - \mathrm{i}\Gamma_{\mathrm{inel}}/2$, the three amplitudes are implemented in a one-channel optical K-matrix form as

$$\mathcal{A}_{\mathrm{FSI}}(E) = \frac{1}{1 - \mathrm{i}kC(E)},$$

$$\mathcal{D}(E) = d(E)[1 - \mathrm{i}kC(E)] - \mathrm{i}kg^2,$$

$$\mathcal{A}_{\mathrm{pole}}(E) = \frac{1}{d(E) - \mathrm{i}kg^2},$$

$$\mathcal{A}_{\mathrm{mix}}(E) = \frac{p_c d(E) + gh}{\mathcal{D}(E)}, \tag{6}$$

where $\Lambda_E = 0.3$ GeV, $p_c = \cos\theta$, and $h = \Lambda_E \sin\theta \mathrm{e}^{\mathrm{i}\phi}$. The constant FSI variant sets $C_1 = 0$, whereas C_1 is fitted in the energy-dependent variant. The constraints $\mathrm{Im}\, C_0 \geq 0$, $C_1 \geq 0$, and $\Gamma_{\mathrm{inel}} > 0$ enforce the absorptive optical convention. All amplitudes are folded with the same phase-space, efficiency, and sideband factors. Fit quality is assessed using the minimum Poisson deviance D, and AICc accounts for the number of fitted parameters; lower values indicate a better fit and a better complexity-adjusted description, respectively. A parametric-bootstrap test is used to compare the energy-dependent FSI and mixed amplitudes.

The fit results are summarized in Fig. 2 and Table 1. Relative to the constant-FSI fit, allowing energy dependence adds one parameter and reduces D from 54.64 to 16.22 and AICc from 61.98 to 26.57. The energy-dependent FSI fit also yields lower values of both quantities than the pole-only fit, for which $n_p = 4$, $D = 24.41$, and AICc = 34.76. It therefore provides the best overall balance between fit quality and the number of parameters. The mixed amplitude achieves a lower deviance, $D = 5.27$, but requires $n_p = 9$ and gives AICc = 38.27, motivating a statistical assessment of whether the reduction in D justifies the additional pole contribution.

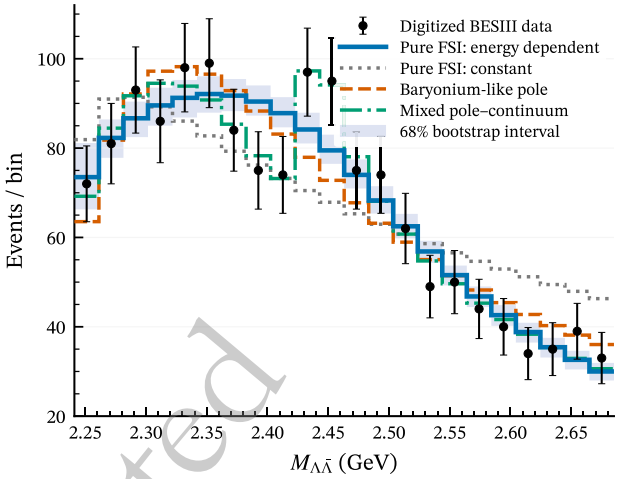


Fig. 2. (color online) Fits to the digitized combined BESIII $M_{\Lambda\bar{\Lambda}}$ spectrum. All curves employ the same response model and sideband treatment. The shaded band denotes the central 68% pointwise interval obtained from the conditional parametric bootstrap of the energy-dependent FSI fit.

Table 1. Fits to the digitized BESIII combined spectrum. Here, n_p denotes the total number of fitted parameters, including the common yield normalization; D is the minimum Poisson deviance; and AICc is the finite-sample-corrected Akaike information criterion.

Model	n_p	D	AICc
Pure FSI: constant	3	54.64	61.98
Pure FSI: energy dependent	4	16.22	26.57
Baryonium-like pole	4	24.41	34.76
Mixed pole–continuum	9	5.27	38.27

We therefore generate 500 Poisson pseudoexperiments under the energy-dependent FSI hypothesis and repeat the model comparison for nine variations of the response, background, fit window, binning, and resolution. The observed $\Delta D = 10.95$ corresponds to $p = 0.048 \pm 0.010$, where the uncertainty is the Monte Carlo standard error. The energy-dependent FSI fit retains the lowest AICc in all tested variations, whereas the mixed fit places Γ_{inel} at the lower limit of its allowed range. The bootstrap result provides only marginal support for the improvement obtained with the mixed amplitude, whereas AICc favors the energy-dependent FSI description. Thus, within the models considered, the digitized spectrum does not provide compelling evidence for an additional explicit-pole contribution.

The preference for the energy-dependent FSI amp-

CPC Accepted

litude is consistent with Haidenbauer and Meißner [26], who evaluated the $\Lambda\bar{\Lambda}$ FSI within the distorted-wave Born approximation using Jülich potentials constrained by $p\bar{p} \to \Lambda\bar{\Lambda}$ data. After an overall normalization, their $^3S_1$ spectra reproduced the near-threshold BESIII mass dependence, providing a dynamically constrained demonstration that an explicit pole is not required to describe the enhancement. Because their study focused on the predictive role of the FSI interaction, it did not, by itself, determine whether the same spectrum allows an additional baryonium component. Our analysis complements their calculation by placing the pure-FSI, explicit-pole, and mixed amplitudes within a common fit and comparing their statistical descriptions of the digitized data.

We also examine whether analytic continuation yields a stable pole position. We define the physical $\Lambda\bar{\Lambda}$ sheet by $\mathrm{Im}\,k > 0$ and the second sheet by $\mathrm{Im}\,k < 0$; in models containing a bare state, the pole is followed continuously from the bare-state limit to the fitted coupling. The energy-dependent FSI amplitude contains a broad second-sheet singularity at $M = 2.420 - \mathrm{i}0.207$ GeV, with 68% bootstrap intervals $\mathrm{Re}\,M = [2.385, 2.441]$ GeV and $\mathrm{Im}\,M = [-0.235, -0.180]$ GeV, whereas the pole continuously connected to the bare state lies at $2.257 - \mathrm{i}0.182$ GeV in the pole-only fit and $2.431 - \mathrm{i}0.014$ GeV in the mixed fit. The variation in both the real and imaginary parts indicates that the present spectrum does not determine a model-independent pole mass and width. This single-channel analysis also does not determine the internal composition of a possible state or its couplings to other channels.

IV. BARYONIUM, QCD SUM RULES, AND MIXING

The fit leaves room for a baryonium contribution, for which the QCD sum-rule prediction provides complementary motivation. Within the narrow-pole approximation, the vector $\Lambda\bar{\Lambda}$ result [17] estimates the mass scale of the lowest-lying physical state that couples to the chosen local hexaquark current. This mass is distinct from the model-dependent parameter M_R in Eq. (5), which is defined before the $\Lambda\bar{\Lambda}$ self-energy correction. The corresponding physical state is associated with a pole of the dressed amplitude. The sum rule therefore motivates a possible state near the BESIII mass region, while the lineshape analysis tests whether the spectrum requires such a contribution. Quantitative matching would require relating the sum-rule mass to the dressed pole through a consistent treatment of the continuum.

A local hexaquark current specifies the quantum numbers of the states to which it couples, but it does not uniquely determine their internal composition. Thus, the physical state, if it exists, may contain both short-distance and hadronic components and can be written schematically as

$$|X\rangle = a|\Lambda\bar{\Lambda}\rangle + b|s\bar{s}\rangle + c|qq\bar{q}\bar{q}\rangle + d|G\rangle + \cdots . \tag{7}$$

A large $|a|^2$ contribution implies enhanced baryon–antibaryon channels and strong sensitivity to $\Lambda\bar{\Lambda}$ FSI. A large $|b|^2$ contribution should be accompanied by conventional strange-meson modes, such as $K\bar{K}$, $K\bar{K}^*$, $K^*\bar{K}^*$, and $\phi\eta$ [27]. Hidden-strange tetraquark or gluonic components would instead favor correlated hidden-strange or multimeson channels [28–30]. Thus, the experimentally relevant question is not whether mixing is present, but which component governs the observed decay hierarchy.

V. FURTHER TESTS: DECAY CHANNELS, POLARIZATION, AND PARTNER STATES

The decay hierarchy discussed above can be tested by comparing baryon–antibaryon and mesonic channels. Combined amplitude analyses can constrain channel couplings and determine whether different spectra share a common pole. Together with angular measurements, these comparisons can further constrain the continuum and pole contributions, whose separation remains model dependent in Section III.

Equation (6) provides qualitative expectations for these tests. In the FSI description, the mass dependence is governed by the continuum interaction and the $\Lambda\bar{\Lambda}$ threshold. In a pole-dominated description, processes that couple to the same state share its pole position, although their observed peak shapes depend on production factors and backgrounds. In the mixed case, interference can enhance or suppress the signal and produce asymmetric peaks or dips as the relative continuum and pole contributions change. These expectations motivate comparisons across processes within a common amplitude analysis. Because FSI can also generate poles, a shared pole position alone does not distinguish a dynamically generated state from an explicit bare-state contribution.

Searches in other $\Lambda\bar{\Lambda}$ partial waves can further test the spin dependence of the interaction. Table 2 lists representative configurations and useful production channels. Whether these configurations support observable partner states depends on the underlying dynamics.

Companion baryon–antibaryon channels and their experimental roles are summarized in Table 3. The $p\bar{p}$ sector provides a benchmark for FSI studies [24]. The $\Sigma\bar{\Sigma}$ and $\Xi\bar{\Xi}$ channels can test correlations suggested by approximate flavor symmetry and coupled-channel dynamics. If the interactions in these channels are related by approximate flavor symmetry, correlated structures may appear near their respective thresholds, with masses and strengths determined by the channel dynamics. Comparing these spectra in similar production processes can test

CPC Accepted

Table 2. Representative $\Lambda\bar{\Lambda}$ baryonium configurations, including the observed 1^{--} channel and possible partner states.

Configuration	Possible J^{PC}	Typical partial wave	Useful probes
$^1S_0$	0^{-+}	S	radiative J/ψ decays; $\eta^{(\prime)}B\bar{B}$ spectra
$^3S_1$	1^{--}	S	$e^+e^- \to \eta\Lambda\bar{\Lambda}$; time-like form factors
$^3P_0$	0^{++}	P	scalar channels and threshold angular distributions
$^1P_1$	1^{+-}	P	spin-dependent angular distributions and associated production channels
$^3P_1$	1^{++}	P	spin correlations in self-analyzing Λ decays
$^3P_2$	2^{++}	P	tensor moments and coupled hyperon-antihyperon channels

Table 3. Companion baryon–antibaryon channels and their role in testing interaction dynamics.

Channel	Diagnostic role	Promising measurements
$p\bar{p}$	FSI benchmark; connection with $X(1835)$	radiative J/ψ decays; form factors
$\Lambda\bar{\Lambda}$	primary channel for $X(2356)$	$e^+e^- \to \eta\Lambda\bar{\Lambda}$ and $e^+e^- \to \Lambda\bar{\Lambda}$
$\Sigma\bar{\Sigma}$	nearby coupled-channel test	scans around hyperon-antihyperon thresholds
$\Xi\bar{\Xi}$	flavor-$SU(3)$ extension	high-statistics BESIII/Belle II data

CPC Accepted

whether a common dynamical description accounts for the observed structures. Such correlations would constrain the interaction, although they would not, on their own, distinguish an explicit state from dynamically generated poles.

Polarization observables provide complementary constraints in the $\Lambda\bar{\Lambda}$ channel. Because the Λ decay is self-analyzing, spin correlations can be measured from the angular distributions of the decay products [22, 31]. If a common scalar FSI or pole factor multiplies all helicity amplitudes, it cancels in normalized spin observables; thus, a mass enhancement need not exhibit a corresponding polarization structure. Conversely, if the continuum and pole terms have different helicity couplings, their interference can produce mass-dependent spin correlations. A joint mass–angular analysis can test this possibility. The scalar amplitudes fitted here do not determine these couplings and therefore do not predict the sign or magnitude of the polarization effects.

VI. CONCLUSION

The $X(2356)$ enhancement lies near the $\Lambda\bar{\Lambda}$ threshold, where final-state interactions can substantially modify the observed spectrum. We have formulated a minimal FSI-dressed pole framework that accommodates pure FSI, baryonium-like pole, and mixed pole–continuum descriptions. Comparison with the digitized BESIII spectrum favors the energy-dependent FSI amplitude when fit quality and model complexity are considered jointly. The mixed amplitude improves the fit, but the statistical support for the additional pole is marginal. The extracted pole positions also vary substantially among models, indicating that the present spectrum does not determine a model-independent pole mass and width.

We have further clarified that the QCD sum-rule prediction concerns the physical mass scale of a possible state and should be distinguished from the bare-state parameter in the line-shape model. Its coupling to a local hexaquark current does not uniquely determine its internal composition, motivating comparisons between baryon–antibaryon and mesonic decay channels. We have identified conditional expectations for continuum–pole interference and spin correlations, together with partner and companion-channel searches that probe the underlying interaction. These complementary measurements can constrain the pole structure, channel couplings, and decay pattern relevant to the baryonium interpretation.

ACKNOWLEDGMENTS

The authors acknowledge the use of Aether (https://aether.aiphys.cn/), an AI agent developed by Peking University, for language editing and manuscript refinement. The authors are fully responsible for the content of this manuscript.

References

[1] C. B. Dover and J. M. Richard, Ann. Phys. **121**, 70 (1979)
[2] I. S. Shapiro, Phys. Rept. **35**, 129 (1978)
[3] J. Cote, M. Lacombe, B. Loiseau *et al*, Phys. Rev. Lett. **48**, 1319 (1982)
[4] O. D. Dalkarov, V. B. Mandelzweig, and I. S. Shapiro,

Nucl. Phys. B **21**, 88 (1970)
[5] W. W. Buck, C. B. Dover, and J. M. Richard, Ann. Phys. **121**, 47 (1979)
[6] L. Montanet, Phys. Rept. **63**, 201 (1980)
[7] C. Amsler, Adv. Nucl. Phys. **18**, 183 (1987)
[8] C. B. Dover, T. Gutsche, and A. Faessler, Phys. Rev. C **43**, 379 (1991)
[9] J. Z. Bai *et al*. (BES Collaboration), Phys. Rev. Lett. **91**, 022001 (2003)
[10] M. Ablikim *et al*. (BES Collaboration), Phys. Rev. Lett. **95**, 262001 (2005)
[11] M. Ablikim *et al*. (BESIII Collaboration), Phys. Rev. Lett. **108**, 112003 (2012)
[12] A. Datta and P. J. O'Donnell, Phys. Lett. B **567**, 273 (2003)
[13] B. S. Zou and H. C. Chiang, Phys. Rev. D **69**, 034004 (2004)
[14] S. L. Zhu and C. S. Gao, Commun. Theor. Phys. **46**, 291 (2006)
[15] M. Ablikim *et al*. (BESIII Collaboration), Phys. Rev. D **88**, 091502 (2013)
[16] S. Q. Zhang and C. F. Qiao, AAPPS Bull. **36**, 12 (2026)
[17] B. D. Wan, S. Q. Zhang, and C. F. Qiao, Phys. Rev. D **105**, 014016 (2022)
[18] B. D. Wan, L. Tang, and C. F. Qiao, Eur. Phys. J. C **80**, 121 (2020)
[19] H. X. Chen, D. Zhou, W. Chen *et al*, Eur. Phys. J. C **76**, 602 (2016)
[20] X. W. Wang, Z. G. Wang, and G. L. Yu, Eur. Phys. J. A **57**, 275 (2021)
[21] M. M. Nagels, T. A. Rijken, and J. J. de Swart, Phys. Rev. D **20**, 1633 (1979)
[22] P. D. Barne *et al*. (PS185 Collaboration), Phys. Rev. C **54**, 1877 (1996)
[23] M. Ablikim *et al*. (BESIII Collaboration), Phys. Rev. D **107**, 112001 (2023)
[24] A. Sibirtsev, J. Haidenbauer, S. Krewald *et al*, Phys. Rev. D **71**, 054010 (2005)
[25] A. I. Milstein and S. G. Salnikov, JETP Lett. **117**, 905 (2023)
[26] J. Haidenbauer and U. G. Meißner, Eur. Phys. J. A **59**, 136 (2023)
[27] M. Piotrowska and F. Giacosa, arXiv: 1708.03175
[28] B. D. Wan and J. C. Yang, Chin. Phys. C **50**, 043104 (2026)
[29] F. X. Liu, X. H. Zhong, and Q. Zhao, arXiv: 2601.03614
[30] F. Giacosa, J. Sammet, and S. Janowski, Phys. Rev. D **95**, 114004 (2017)
[31] B. Aubert *et al*. (BABAR Collaboration), Phys. Rev. D **76**, 092006 (2007)

CPC Accepted